Uncovering heterogeneity of local lattice distortion in TiZrHfNbTa refractory high entropy alloy by SR-XRD and EXAFS

Yuan-Yuan Tan [a,†], Tong Li [a,b,†], Yu Chen [c], Zhong-Jun Chen [c], Ming-Yao Su [a,b], Jing Zhang [c], Yu Gong [c], Tao Wu [d], Hai-Ying Wang [a,b], Lan-Hong Dai [a,b,e,*]

[a] State Key Laboratory of Nonlinear Mechanics, Institute of Mechanics, Chinese Academy of Sciences, Beijing 100190, P R China
[b] School of Engineering Science, University of Chinese Academy of Sciences, Beijing 100049, P R China
[c] Institute of High Energy Physics, Chinese Academy of Sciences & Graduate, University of Chinese Academy of Sciences, Beijing 100049, P R China
[d] Zhejiang Institute of Mechanical & Electrical Engineering, Hangzhou 310053, P R China
[e] State Key Laboratory of Explosion Science and Technology, Beijing Institute of Technology, Beijing 100081, P R China

ARTICLE INFO

ABSTRACT

Local lattice distortion is usually hypothesized to be severe in TiZrHfNbTa refractory high entropy alloy (RHEA). However, few works have made to quantitatively evaluate element specified distortion and its effect on mechanical behavior of this alloy. In this work, we herein provide a quantitative assessment of element specified local lattice distortion in both the as-prepared and tested TiZrHfNbTa RHEA using a combination of X-ray diffraction and extended X-ray absorption fine structure spectrum (EXAFS). The results show a more significant local lattice distortion ($5.2 \pm 0.3\%$) around Zr-center than that ($4.0 \pm 0.4\%$) around Nb-center in the as-prepared TiZrHfNbTa RHEA, and the distortion magnitude become more prominent after tensile test. Splitting features are observed in the Fourier transformed EXAFS spectra due to heterogeneous atom motions during deformation. The underlying mechanisms of this element-specified local distortion and its influence on solid solution hardening and ductility degradation are discussed as well.

TiZrHfNbTa refractor high-entropy alloy (RHEA) has recently emerged as promising candidate for high-temperature structural applications [1–2] due to high strength and ductility. Local lattice distortion, tightly relating to individual alloying components, is proposed to play a key role in solid solution hardening of TiZrHfNbTa RHEA [3–5]. Although, local lattice distortion in body center cubic (BCC) structured TiZrHfNbTa RHEA is often hypothesized to be much more significant than that of face center cubic (FCC) structured CrMnFeCoNi (Cantor) HEAs [5–8], few experimental works have been conducted on direct comparisons of their local lattice distortion degrees due to limited methods. The lacking of quantitative assessment of element specified local lattice distortion leads to controversial viewpoints on contributions of local lattice distortion to mechanical behavior. Wang et al. [9] showed that alloying Hf into NbTa solution would manifests a much higher strengthening potency than Ti. While, addition of Zr to NbTa base greatly reduces the ductility [10]. Nevertheless, higher content of Zr in bulk metallic glasses favors a higher ductility [11]. For RHEAs, Senkov et al. [1] replaced W, Mo and V with Hf, Zr and Ti, and thus obtained the

extensively studied TiZrHfNbTa alloy with high ductility. Based on our studies [8,12,13] of Cantor alloys, the local lattice distortions closely relate to atomic size misfit, and it should be heterogeneous in TiZrHfNbTa RHEA due to a larger atomic size misfit. Profound understanding of element specified local lattice distortion in TiZrHfNbTa RHEA would save time on composition tailoring.

However, it is not easy to interpreting factors that causing local lattice distortion due to difficulties in accurate estimation of atomic size. Thirathipviwat et al. [14] consider atomic size misfit is one of the foremost contributions, while Meng et al. [15] demonstrate that electron transfer produces variations in local lattice distortion magnitude. Our studies indicate a reduction of local lattice severity due to charge transferring in Cantor alloy [8]. Recent atomistic simulations have discussed the correlations among local lattice distortion and other properties associated with the charge transfer and electronegativity [16]. The local electronic structure evolution of the constitute elements during alloying would change the size of electron cloud and thus vary the lattice distortion. Finding another parameter that has no necessity to
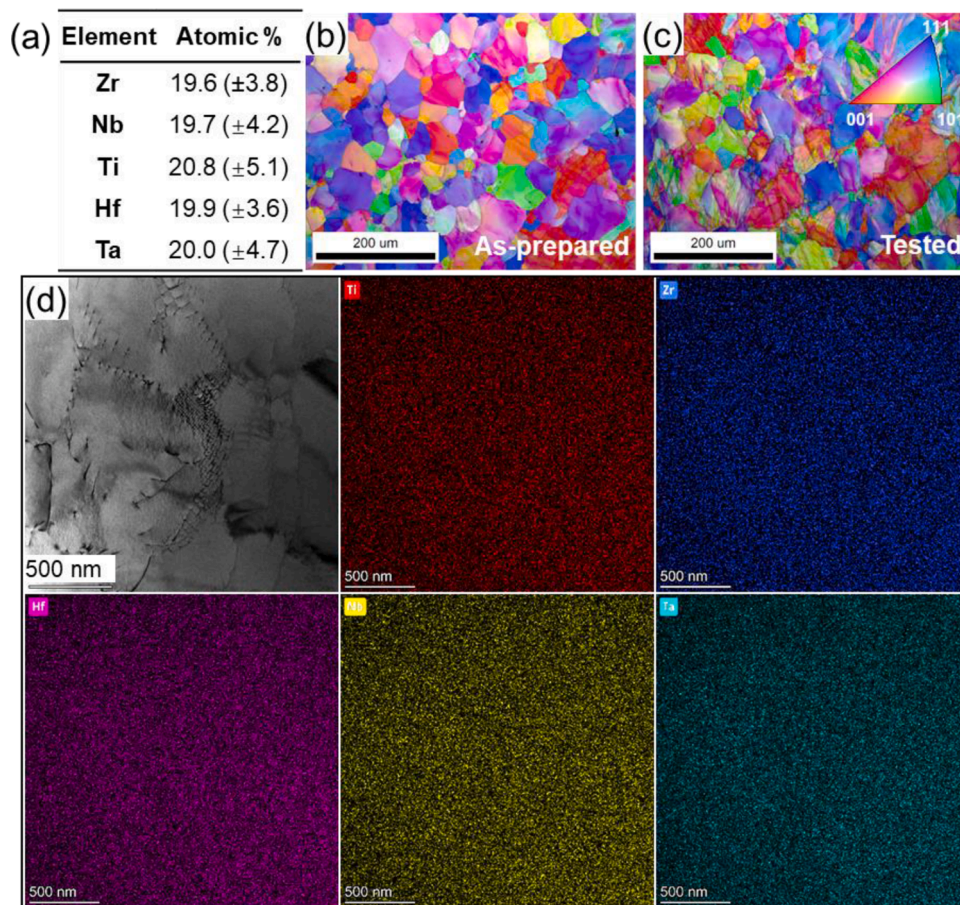
Fig. 1. (a) Chemical composition obtained from EDS spectra. (b) IPF image of as-prepared TiZrHfNbTa RHEA without deformation. (c) IPF image nearby the fracture part of a tested TiZrHfNbTa RHEA. (d) EDS mapping of the as-prepared TiZrHfNbTa RHEA.

obtain exact atomic radius should be an alternative option. To quantitatively evaluate element specified local lattice distortion in TiZrHfNbTa RHEA and explore its correlations with mechanical performance, a combination of appropriate experiment methods is the key.

The frequently used methods on quantifying local lattice distortion are synchrotron radiation-based X-ray diffraction (SR-XRD), neutron scattering, pair distribution function (PDF), high resolution transmission electron microscope (HRTEM) and extended X-ray absorption fine structure spectrum (EXAFS) [17]. The averaged lattice parameter could be obtained using Rietveld refinement of a full SR-XRD pattern, and subsequently the averaged atom pair distance $\bar{r}$. For the high quality of SR-XRD dataset, local lattice distortion could be extracted from the Bragg peak decay. By fitting across the entire r-range of a PDF spectrum, it is possible to estimate local lattice distortions in a relatively longer atomic range, as well as $\bar{r}$. The EXAFS spectrum allows direct probing of atom pair distance around specific element atoms, potentially providing element specified local lattice distortions. SR-XRD, PDF and EXAFS datasets generate both temporally and spatially averages, making these results more statistical significance. Using only SR-XRD or PDF are difficult to capture element specified local structure evolutions. EXAFS data set only could provide local coordination environment including coordinated atom type and number, bond distance and local chemical environments. But the averaged atom pair distance it provides is not superior to SR-XRD and PDF. Whereas, the HRTEM is capable of yielding high resolution images of atomic columns in a material, the atomic size and atom pair distance are possible to be measured. However, the sample preparation is much more difficult, and it's not easy to exclude the effects of sample thinning and electron beam heating. We thus propose to assess local lattice distortion in TiZrHfNbTa RHEA using a

combination of SR-XRD and EXAFS [8]: extracting averaged atom pair distance $\bar{r}$ from SR-XRD pattern, meanwhile, obtaining element specified atom pair distance from EXAFS spectra. Subsequently, element specified local lattice distortion could be calculated using Eq. (1),

$$\chi_i = \sqrt{\sum_j^n C_j \left(1 - \frac{r_{i-j}}{\bar{r}}\right)^2} \times 100\% \tag{1}$$

where χ_i is local lattice distortion centered around i atom, r_{i-j} the atom pair distance from j to i, $\bar{r}$ the averaged atom pair distance calculated from lattice parameter a, and C_j the atomic content of j element atoms. In this method, we use atom pair distances from experiment datasets, no need for theoretical evaluation of atomic radius.

Bulk TiZrHfNbTa alloy are prepared by arc melting of counterpart pure metals (purity >99.99%) in Ar atmosphere. Air cooling, homogenization, hot-rolling, cold-rolling, and annealing are processed in sequence. Dog-bone-shaped tensile sample, tested (MTS-810 standard) at a constant strain rate of $5 \times 10^{-4}\ s^{-1}$, shows a yield strength of ~1100 MPa and a fracture strain of ~14% in Fig. S1 (a). Electron backscatter diffraction pattern (EBSD) and Energy-dispersive X-ray spectroscopy (EDS) are collected using JEOL JSM-7900F to characterize chemical compositions and microstructure in Fig. 1(a), (b) and (c). Similar grain size and orientation are observed in the as-prepared and tested samples (Fig. S1 (b) and (c)), respectively. Twin-jet electropolisher is conducted to collect EDS mappings (Titan Cubed G2 60 at 300 kV) of the as-prepared TiZrHfNbTa RHEA. The results in Fig. 1(d), S2 (a) and (b) show no obvious element aggregate.

Two TiZrHfNbTa RHEA samples (as-prepared and tested) with a thickness of ~60 μm are prepared. The tested one is cut from the fracture part of the dog-bone-shaped tensile sample. SR-XRD patterns are
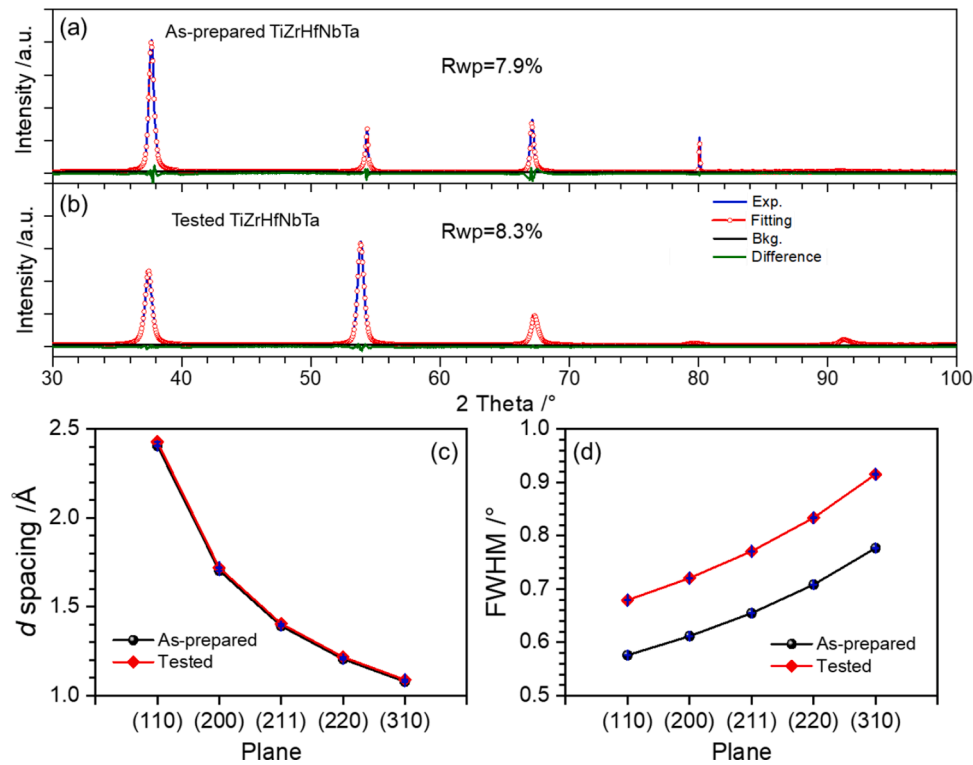
Fig. 2. (a) XRD patterns and the corresponding fitting details of as-prepared (a) and tested (b) TiZrHfNbTa RHEA. The dotted fitting line skipped three points to make the experiment patterns observed. (c) The calculated *D*-spacing values and the (d) full width at half maximum (FWHM) of the as-prepared and tested samples. The error bars are shown in blue.

collected at 1W1A beamline in Beijing Synchrotron Radiation Facility with an incident wavelength of λ=1.5438 Å, a 2theta range from 30 to 100° with a scan step of 0.02°. Transmitted EXAFS spectra from *K*-edges of Zr and Nb are measured at 1W1B beamline. Transmitted EXAFS spectra of Zr and Nb foil are collected at the same time to estimate amplitude attenuation factor S_0^2 for EXAFS fitting analysis. Fluorescence EXAFS spectra from *K*-edges of Ta and Hf are measured at 4B9A beamline, and that of Ta foil for self-absorption effect correction

evaluation. Demeter software package [18] is used for XANES normalization and EXAFS fitting with some constraints [19].

Both of the as-prepared and tested TiZrHfNbTa RHEA samples hold typical BCC structure in Fig. 2(a) and (b). The Rietveld refinement and line profile fitting analysis are conducted using High Score suite [20]. The peak profile is modeled by a Pseudo-Voigt function corrected for asymmetry owing to axial divergence. The full width at half maximum (FWHM) of diffraction peak is calibrated using standard Si powder
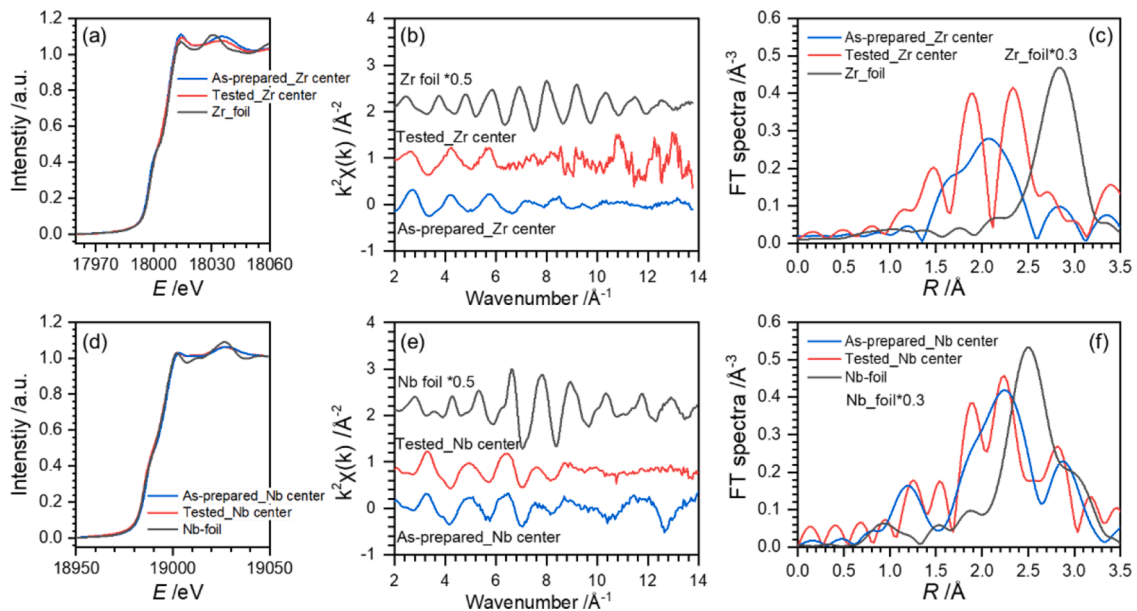

Fig. 3. XANES spectra, extracted k^2-weight EXAFS spectra and Fourier transformed EXAFS spectra without phase corrections (a-c) from the Zr *K*-edge and (e-g) from Nb *K*-edge of as-prepared and tested TiZrHfNbTa RHEA, respectively.
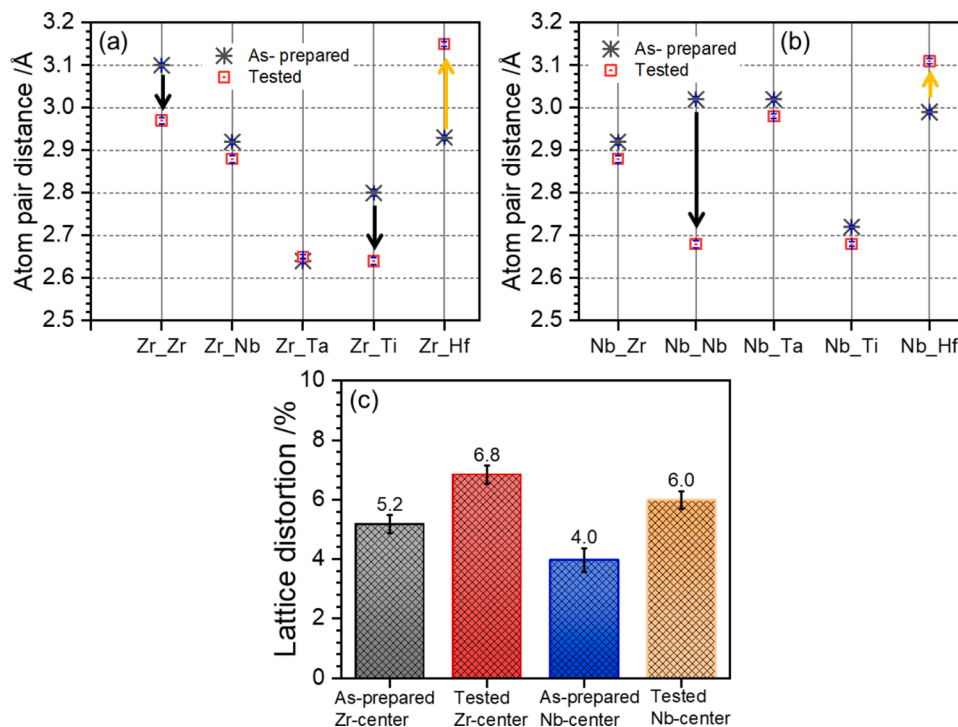
Fig. 4. Atom pair distance evolutions around (a) Zr-center and (b) Nb-center in TiZrHfNbTa RHEA from the as-prepared state to after tensile test (tested state). Error bars are presented in blue. (c) Comparison of local lattice distortions around Zr-center and Nb-center in the as-prepared and tested TiZrHfNbTa RHEA. Error bars are presented in black.

sample measured at the same condition. The preferred orientations are refined using March-Dollase function with caution. A slight low-angle side shift of the diffraction peaks in Fig. 2(b) compared with that in Fig. 2(a), which indicates variations of Type I and Type II strains [21]. The obtained lattice parameters are $a = 3.4158(2)$ Å and $a = 3.4506(3)$ Å for the as-prepared and tested samples, respectively. The measured lattice parameter of the as-prepared sample is 0.007 Å larger than the calculated one (3.409 Å) in accordance with Vegard's law [1,22]. This slight positive deviation has been observed in binary alloy system [23], and is proposed as an indicate of random distribution of alloying elements in the TiZrHfNbTa RHEA [1]. Meanwhile, the result agrees well with the EDS mappings in Fig. 1(d) and thus justifies the equiatomic constraint in EXAFS fitting. The interplanar spacing for individual planes increases overall as well in Fig. 2(c). FWHM broadening in Fig. 2 (d) implies a rise of Type III strains, as well as local lattice distortions, in the deformed sample. The variation of diffraction peak intensity after deformation manifesting a local lattice strain increase on (110) plane and a reduction in (200) plane, which will be further explored from EXAFS results in the following.

Fig. 3 shows comparison of EXAFS spectra from Zr and Nb *K*-edge of as-prepared and tested TiZrHfNbTa RHEA with those of standard Zr and Nb foils. The well overlapping of XANES spectra above the absorption edge in Fig. 3(a) indicates similar local electric structure of Zr in TiZrHfNbTa RHEA and standard Zr foil. However, the afterward differences in oscillation amplitude and frequency imply variations in local coordination structures around Zr-center among the three alloys. The differences are more clearly presented in extracted k^2-weight EXAFS spectra in Fig. 3(b). After Fourier transformation in Fig. 3(c), one broad main coordination peak with a shoulder is observed for the as-prepared sample, probably due to a limited *k* range (0–13.6 $Å^{-1}$). But this broad peak split into two sharp ones after test, which manifests re-ordering of atoms around Zr center. Noticeably, the coordination peak positions in Fig. 3(c) demonstrate a shorter averaged atom pair distance centered around Zr in TiZrHfNbTa RHEA than that in Zr foil.

The high similarity of XANES spectra in Fig. 3(d) in the above edge

range manifests local electronic structures of the three samples are alike, which is quite different from the Cantor alloys [8]. This also indicates little atomic size change caused by electron charge transfer in TiZrHfNbTa RHEA. The deviation after white line peak in Fig. 3(d) suggests slight differences of local coordination structure between the as-prepared and tested TiZrHfNbTa RHEAs. However, the oscillation amplitude of XANES spectra from TiZrHfNbTa RHEAs are much weaker than that of standard Nb foil, resulting from the difference of local coordination environments such as element type, atom pair distance, and coordinated atom number. The extracted k^2-weighted EXAFS spectra in Fig. 3(e) further verify this point in mismatches of oscillation frequency and amplitude. The averaged atom pair distance around Nb center in TiZrHfNbTa RHEAs in Fig. 3(f) is shorter (about 0.3 Å) than that of Nb foil, and hence indicating a lattice shrinkage compared with Nb foil. The splitting feature illustrates a re-ordering of coordination atoms from a broader local atom pair distance distribution to two distinguishable shells. Some atoms become closer to the Nb and Zr centers, while, others go far away, corresponding to the first and second nearest neighbor shell in the coordination configuration of a typical BCC structure. The differences in atom movements would possibly form some ordered clusters, such as preferred orientation as presented in Fig. 2(b).

To clarify the heterogeneous atom motions during tensile deformation, EXAFS fitting analysis is carefully conducted with constraints due to a limited *k* range. Firstly, equiatomic confinement is applied according to the EDS mapping and SR-XRD results. Then, the same edge energy shifts parameter and Debye-Waller factor variable are used to all the fitted shells in accordance with the similarity of XANES feature and extracted EXAFS oscillation. These constraints make the EXAFS fittings with five shells possible in a limited *k* range of 2.4–13.6 $Å^{-1}$ and *R* range of 1.4 to 3.6 Å. The S_0^2 is set as 0.91 based on EXAFS fittings of standard Zr and Nb foil. The fitting details and results are shown in Fig. 4, Fig. S3, and Table S1. In a standard Nb foil with a BCC structure, the first shell consists of 8 Nb atoms with a distance of 2.88 Å, and the second shell has 6 with a distance of 3.33 Å [24]. Although it is difficult to classify the atom pair distance distribution in Fig. 4(a) into to two shells due to a
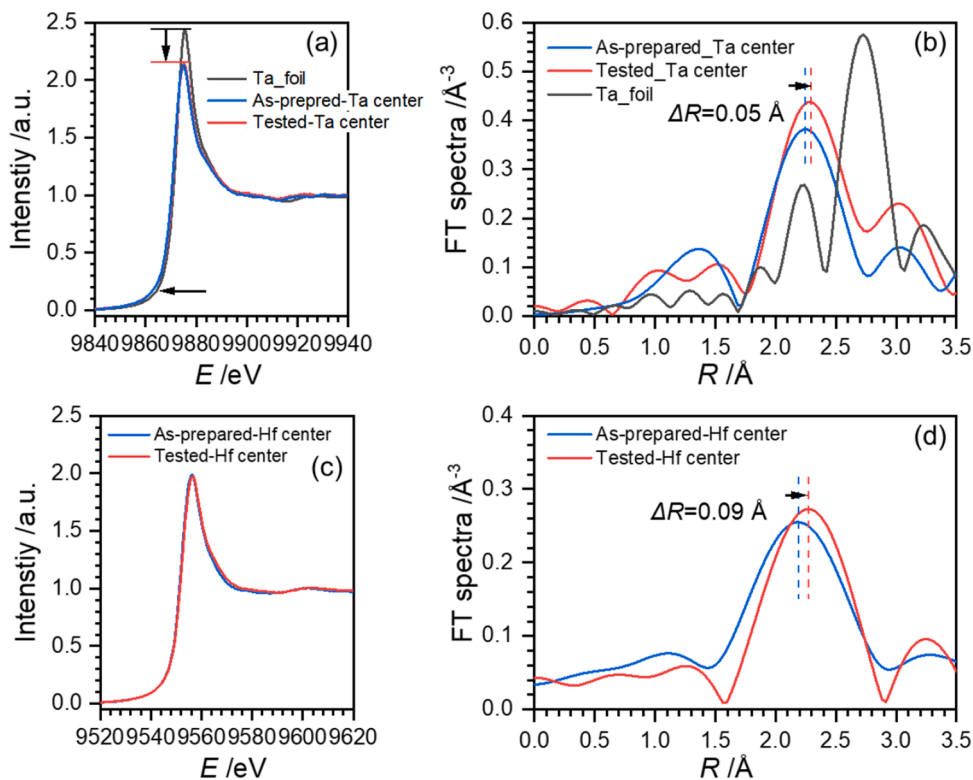
Fig. 5. XANES spectra and Fourier transformed EXAFS spectra (a, b) from the Ta *K*-edge and (c, d) from Hf *K*-edge of as-prepared and tested TiZrHfNbTa RHEA, respectively.

relatively uniform interval, we see clearly that Ta and Ti atoms are near the Zr center, while, Zr, Nb and Hf atoms are far away from the center. In contrary, only Ti atoms are found to be closer to Nb center in Fig. 4(b). However, this ranking becomes more evident after tensile test as demonstrated by the hollow square marks in Fig. 4(a) and (b). This result potentially illustrates that atoms with larger atomic radius are in favor of going to outer shell, while, smaller atoms are fond of staying in the inner shell during tensile test.

We quantitatively evaluate local lattice distortion around Zr-center and Nb-center using Eq. (1). The results give a χ_i of $(5.2 \pm 0.3)\%$ around Zr-center in the as-prepared TiZrHfNbTa RHEA in Fig. 4(c), approaching to the solid solution limit of ~6.6% [21] [25] in binary solid solutions. However, this value reaches to 6.8% after tension test, and the sample still keeps in a single BCC phase. But we should keep in mind that the χ_i is calculated from averaged atom pair distance, while, the limit value comes from the theoretical atomic radius. The χ_i around Nb-center is $(4.0 \pm 0.4)\%$, close to the local lattice distortion around Ni-center in CrMnFeCoNi HEA [8]. In TiZrHfNbTa RHEA, larger atoms, Zr, hold a more profound local lattice distortion, while, smaller atoms, Nb, present a moderate local lattice distortion. Possibly, this is the reason that a more prominent solid-solution hardening is observed for alloying Zr. The increases of local lattice distortion magnitude after tensile test, probably, resulting from dislocation and twinning activities.

Unfortunately, it is difficult to collect transmitted EXAFS spectra from the Ta and Hf *K*-edges due to experiment condition confinements. We therefore collected EXAFS spectra as long as possible in fluorescence mode to simply explore atom pair distance evolution. However, we do not obtain desirable self-absorption (SA) effect corrections even using standard Ta foil as shown in Fig. S4, S5 and S6. The SA effect has greatly reduced the oscillation amplitude of EXAFS spectra, but it has little impact on the position of coordination peak. Therefore, we could roughly compare the atom pair distance evolution using EXAFS spectra. The XANES spectra from the Ta and Hf *K*-edges of as-prepared and tested TiZrHfNbTa RHEA in Fig. 5(a) and (c) present little variations, although

the white line peak of TiZrHfNbTa RHEA is much lower than that of Ta foil in Fig. 5(a). The averaged atom pair distance around Ta-center becomes about 0.05 Å longer in Fig. 5(b) after tensile test, and that of Hf-center goes a 0.09 Å elongation. We further calculated the changes of averaged atom pair distance around Zr-center and Nb-center, and get a -0.06 Å and -0.05 Å shortening after tensile test. This shows clearly that the averaged atom pair distance around larger atoms would go through a longer distance under the same deformation. Probably, the bond interactions centered around larger atoms are weaker than that around smaller atoms, thus making the atom pair distance easier to be elongated. However, this elongation probably has little good to plasticity.

In summary, we combine SR-XRD and EXAFS methods to elucidate element specified local lattice distortion in TiZrHfNbTa RHEA before and after tensile test. The XANES spectra reveal little charge transfer among alloying compositions in TiZrHfNbTa RHA. An interesting co-ordination shell splitting is observed in the EXAFS spectra after tensile test due to heterogeneous atom motions. The results demonstrate a more significant local lattice distortion around Zr than that around Nb centers in the as-prepared TiZrHfNbTa RHEA, and become more prominent after tensile test.

Declaration of Competing Interest

The authors declare that they have no known competing financial interests or personal relationships that could have appeared to influence the work reported in this paper.

Acknowledgments

Supplementary materials

Supplementary material associated with this article can be found, in the online version, at doi:10.1016/j.scriptamat.2022.115079.

References

[1] O.N. Senkov, J.M. Scott, S.V. Senkova, D.B. Miracle, C.F. Woodward, J. Alloys Compd. 509 (2011) 6043–6048.

[2] C. Lee, G. Kim, Y. Chou, B.L. Musicó, M.C. Gao, K. An, G. Song, Y.C. Chou, V. Keppens, W. Chen, P.K. Liaw, Sci. Adv. 6 (2020).

[3] C. Lee, Y. Chou, G. Kim, M.C. Gao, K. An, J. Brechtl, C. Zhang, W. Chen, J. D. Poplawsky, G. Song, Y. Ren, Y.C. Chou, P.K. Liaw, Adv. Mater. 32 (2020) 1–9.

[4] L. Li, Q. Fang, J. Li, B. Liu, Y. Liu, P.K. Liaw, Mater. Sci. Eng. A 784 (2020).

[5] Y. Tong, S. Zhao, H. Bei, T. Egami, Y. Zhang, F. Zhang, Acta Mater 183 (2020) 172–181.

[6] H. Song, F. Tian, Q.M. Hu, L. Vitos, Y. Wang, J. Shen, N. Chen, Phys. Rev. Mater. 1 (2017) 1–8.

[7] L.R. Owen, E.J. Pickering, H.Y. Playford, H.J. Stone, M.G. Tucker, N.G. Jones, Acta Mater 122 (2017) 11–18.

[8] Y.Y. Tan, M.Y. Su, Z.C. Xie, Z.J. Chen, Y. Gong, L.R. Zheng, Z. Shi, G. Mo, Y. Li, L. W. Li, H.Y. Wang, L.H. Dai, Intermetallics 129 (2021), 107050.

[9] S.P. Wang, E. Ma, J. Xu, Intermetallics 107 (2019) 15–23.

[10] H.Z. Li, J. Xu, J. Mech. Behav. Biomed. Mater. 32 (2014) 166–176.

[11] H. Wang, W. Dmowski, Y. Tong, Z. Wang, Y. Yokoyama, J. Ketkaew, J. Schroers, T. Egami, Phys. Rev. Lett. 128 (2022), 155501.

[12] Y.Y. Tan, Z.J. Chen, M.Y. Su, G. Ding, M.Q. Jiang, Z.C. Xie, Y. Gong, T. Wu, Z. H. Wu, H.Y. Wang, L.H. Dai, J. Mater. Sci. Technol. 104 (2022) 236–243.

[13] Y.Y. Tan, M.Y. Su, Y.Y. Niu, Z.C. Xie, Z.J. Chen, Y. Gong, J.X. Chen, Z.H. Wu, H. Y. Wang, P.K. Liaw, L.H. Dai, J. Mater. Res. 36 (2021) 4413–4425.

[14] P. Thirathipviwat, S. Sato, G. Song, J. Bednarcik, K. Nielsch, J. Jung, J. Han, Scr. Mater. 210 (2022), 114470.

[15] F. Meng, W. Zhang, Z. Zhou, R. Sheng, A.C.P. Chuang, C. Wu, H. Huang, S. Zhang, H. Zhang, L. Zhu, L. Jiang, P.K. Liaw, S. Chen, Y. Tong, Scr. Mater. 203 (2021), 114104.

[16] Y. Shiihara, Y. Itai, I. Lobzenko, T. Tsuru, Front. Mater. 9 (2022) 1–10.

[17] L.R. Owen, N.G. Jones, Scr. Mater. 187 (2020) 428–433.

[18] B. Ravel, M. Newville, J. Synchrotron Radiat. 12 (2005) 537–541.

[19] B. Ravel, J. Phys. Conf. Ser. 190 (2009).

[20] T. Degen, M. Sadki, E. Bron, U. König, G. Nénert, Powder Diffr 29 (2014) S13–S18.

[21] L.R. Owen, N.G. Jones, J. Mater. Res. 33 (2018) 2954–2969.

[22] E. Zen, Validity of "Vegard's Law" (1956) 5–6.

[23] K.Q. Lu, Z.H. Wu, J. Dong, X.P. Chen, Z.Z. Fang, Sci. China A 4 (1992) 390–397.

[24] H.G. Schimmel, J. Huot, L.C. Chapon, F.D. Tichelaar, F.M. Mulder, J. Am. Chem. Soc. 127 (2005) 14348–14354.

[25] Y. Zhang, T.T. Zuo, Z. Tang, M.C. Gao, K.A. Dahmen, P.K. Liaw, Z.P. Lu, Prog. Mater. Sci. 61 (2014) 1–93.